Determination of the nozzle flow now requires simultaneous solution of Eqs (4, 10, and 14) for $\overline{\delta_1}$, $\overline{\delta_2}$, and u These equations are closely related to the ordinary boundary-layer integral equations; however, while u (the external velocity) is usually known, the nozzle problem is complicated by the fact that the variation of u_e is itself dependent upon the solution of Eqs (10) and (14) since u_e must satisfy Eq (4) for the conservation of mass

In the turbulent case it will generally be necessary to introduce empirical assumptions regarding the velocity distribution through the boundary layer and the skin friction coefficient The energy equation may be replaced by the assumption that Crocco's relation between velocity and enthalpy is valid

References

[1] Schlichting, H , "Berechnung der Strömung in rotationsymmetrischen Diffusoren mit Hilfe der Grenzschicht-theorie," Z Flugwissenschaften 9, n 4/5 (1961)

[2] Durand, J A and Potter, J L , "Calculation of thicknesses of laminar boundary layers in axisymmetric nozzles with low density, hypervelocity flows," Arnold Eng Dev Center, AEDC-TN-61-146 (December 1961)

[3] Michel, R , "Developpement de la couche limite dans une tuyere hypersonique," *AGARD Specialists Meeting High Temperature Aspects of Hypersonic Flow, Rhode Saint Genese, Belgium* (Pergamon Press Ltd , London, 1963)

[4] Burke, A F and Bird, K D , "The use of conical and contoured expansion nozzles in hypervelocity facilities," *Proceedings of Second Symposium on Hypervelocity Techniques; Advances in Hypervelocity Techniques* (Plenum Press, New York, 1962), pp 373–424

[5] Sichel, M , "The effect of the boundary layer upon the flow in a conical hypersonic wind tunnel nozzle," Univ Mich , Office of Res Administration Rept 02953-2-F (July 1963)

[6] Schubauer, G B and Tchen, C M , "Turbulent flow," *High Speed Aerodynamics and Jet Propulsion; Turbulent Flows and Heat Transfer*, edited by C C Lin (Princeton University Press, Princeton, N J , 1959), Vol V

[7] Shapiro, A H , *The Dynamics and Thermodynamics of Compressible Fluid Flow* (Ronald Press, New York, 1954), Vol II, p 1092

A Simple Geometric Method for Analyzing Polarization States in Photoelasticity

ROBERT MARK*

Princeton University, Princeton, N J

IN the photoelastic model analysis of thin shells such as those employed for typical rocket structures, it is frequently necessary to account for the effect of rotating principal stress axes through the shell wall in regions where the principal shell membrane forces are not acting along the same axes as the principal bending moments The procedure described in this note, which has had important application in the field of crystal-optics[1] and electrical engineering,[2] can be utilized to give particular solutions for the shell problem, as well as providing clear understanding of other polarization phenomena observed in general photoelasticity

Linearly polarized light passing through the strained birefringent element shown in Fig 1 is split into components along the principal stress axes x, and y The field E_y is seen to lead E_x by the phase difference $\delta\lambda$, since the propagation velocity through the strained element along the y-principal stress axis is greater than that of the component along the

Received October 7, 1963

* Lecturer, Department of Civil Engineering

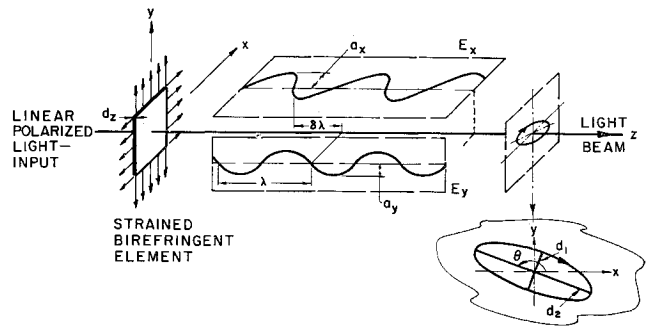

Fig 1 Polarization output from a strained birefringent element

x axis In this case, the y axis is referred to as the fast axis of the element

The ratio of the amplitudes of the field components a_x, a_y depends on the orientation of the element with respect to the polarizing axis; the phase difference is a function of the wavelength of the light employed, material properties and thickness of the element dz, and the principal stress differences along the light path These relationships are derived in standard photoelasticity texts

Resolution of the components along the light beam z axis at a particular instant forms a helix which when viewed from the outer end of the beam is seen as an ellipse The "elliptical" polarization thus formed is defined as "right-handed" if the helix has the form of a right-handed screw thread, and left-handed if it is of the opposite hand

The state of polarization may be completely described by giving its handedness along with the azimuth of the major

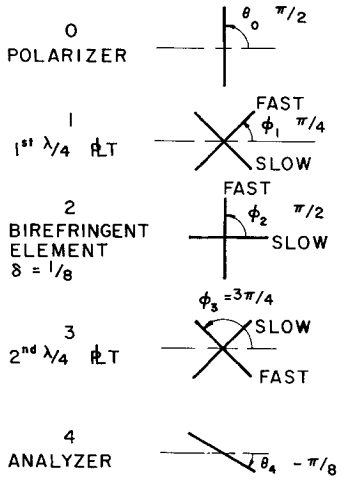

Fig 2a Arrangement of circular polariscope for tardy compensation

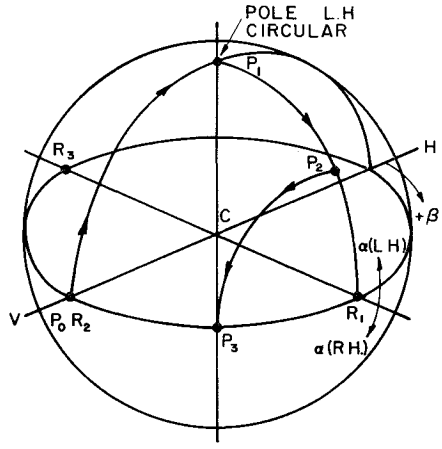

Fig 2b Poincaré sphere solution of Fig 2a

axis of the ellipse θ and the ratio of its semiaxes d_1/d_2, known as its ellipticity Furthermore, it can be shown that these parameters can be represented by points on the surface of a sphere of unit radius[3] and that each point on the spherical surface uniquely represents a particular polarization state P The sphere, due to Poincaré (1892), is shown in Fig 2b

Latitude α is related to ellipticity and handedness by

$$\tan\frac{\alpha}{2} = \frac{d_1}{d_2} \tag{1}$$

where α is positive for left-hand polarization and negative for right-hand polarization Thus, the equator represents a degeneration of the ellipse to linear polarization $d_1/d_2 = 0$ and the poles represent circular polarization $d_1/d_2 = 1$

Longitude β is related to the azimuth of the ellipse by

$$\beta = 2\theta \tag{2}$$

with positive sign convention shown in Fig 2b

Operation of the Sphere

The power of the Poincaré sphere lies in its ability to predict the effect of a series of birefringent elements on polarized light The sequence of sphere operation for each element in the series is given by:[4]

1) The known polarization input P_{n-1} acting on the nth element is plotted as a point on the sphere surface as previously outlined

2) A second point R_n is plotted on the equator with $\beta_{Rn} = 2\phi_n$, where ϕ_n represents the orientation of the fast axis of the element

3) Rotate the sphere $2\pi\delta_n$ about a radial vector drawn through R_n such that an observer on the outside portion of the vector observes a clockwise trace on the sphere beginning at P_{n-1}

The end of the trace represents the output polarization state from the element and it may be used directly as P_n for the next operation This process will be clarified by considering the example below

Circular Polariscope

The standard arrangement of a circular polariscope, shown schematically in Fig 2a, is set up for the analysis of a birefringent element having a principal axis aligned with the polarizer axis and a retardation of $\lambda/8$ The polarized light solution is plotted on the sphere in Fig 2b The output from the second quarter-wave plate is seen to be linear and has its azimuth $\theta_3 = 3\pi/8$ The analyzer can then be rotated to $\theta_4 = -(\pi/8)$ to achieve complete extinction agreeing with well known results of tardy compensation The reader may wish to confirm, by similar analysis, that when a

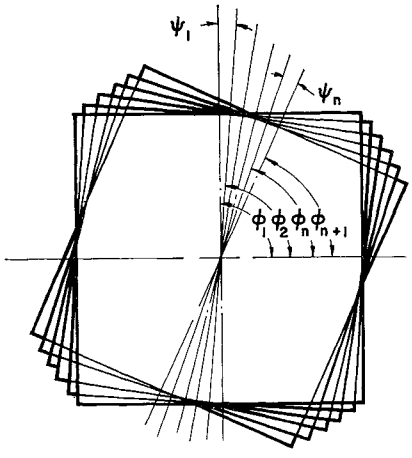

Fig 3 Birefringent elements representing shell wall

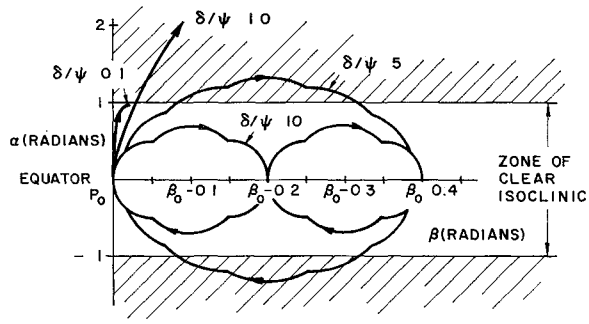

RESULTS

OUTPUT FROM STACK OF 9 SKEWED ELEMENTS			
δ/ψ	POLARIZATION STATE θ(RADIANS)	d_1/d_2	ISOCLINIC EXTINCTION POSSIBLE
0 1	θ_0 .01	.05	YES
1.0	ELLIPTICAL		NO
5	θ_0	0	YES
10	θ_0	0	YES

Fig 4 Modified Poincaré sphere

principal stress axis of the model is not aligned with the polarizer axis, the output from the second quarter-wave plate is elliptically polarized and that complete extinction is not possible, a phenomenon often experienced by the photoelastician

Rotating Stress Field in a Thin Shell

The effect of rotation on polarization states of light passing through a shell wall can be examined by considering the wall to be composed of a series of skewed birefringent elements as shown in Fig 3 The output from the stack of plates is then equivalent to that of the shell

As an example of this approach, consider the problem of a rotated isoclinic in a thin shell Examination of an isoclinic in a single element is performed by aligning a principal stress plane with the axis of the polarizer and observing extinction of the linear polarization passing through the element with the crossed polariscope analyzer When observing a series of skewed elements, one would expect a rotated isoclinic to be developed and, hence, that it would not be observed merely by crossing the analyzer A possible solution to eliminate this difficulty could be the use of a reflecting polariscope with a reflecting surface below the pile of elements Here the optic axes of both the first and last optical elements in the reflecting pile are aligned so that isoclinics might be observed in the usual manner The validity of this approach may be evaluated by means of the Poincaré sphere

In general, the rate of principal stress rotation through the wall of a shell is not constant However, to simplify this application, we will consider only examples of constant rotation $(\delta/\psi) = C$ A further simplification can be employed by observing that we are concerned here only with isoclinic analysis which implies states of linear or near-linear polarization $d_1/d_2 \rightarrow 0$ † As these are located in the region of the equator on the sphere, our solution may be plotted on a linear approximation of the developed equator region shown in Fig 4

All the solutions plotted on Fig 4 are based on a total angle of rotation of the stack of elements $(\Sigma\psi) = 0\,2$ rad and the use of a reflecting surface, hence the presence of ascending and descending traces Individual solutions are based on constant δ/ψ values of 10, 5, 1 0, and 0 1

The results indicate that elliptical polarization may be produced over intermediate ranges of the parameter δ/ψ and that the proposed isoclinic viewing techniques would not function in this range These conclusions are substantiated by the work of Mindlin and Drucker[5 6] for the higher range

† Isoclinic interference is experimentally observed for values up to $d_1/d_2 = 0\,05$ ($\alpha = 0\,1$)

of ζ/ψ and by Franz and Teepe[7] using very low values of ζ/ψ Experimental confirmation also can be obtained from analyzing a stack of skewed quarter-wave plates cut from Polaroid quarter-wave plastic sheet

Complete light-solutions for the general shell problem may be obtained with a train of matrices performing the operations of the sphere [4] The value of the approach outlined here is that a clear visual conception of complex polarization states is readily achieved; hence, the method of the sphere may be quite useful in helping to formulate approaches for final mathematical solutions

References

[1] Ramachandran, G N and Ramasehon, S , "Crystal optics," *Handbuch der Physics*, Band XXV/1, edited by S Flugge (Springer-Verlag, Berlin, 1961), pp 1–217

[2] Deschamps, G A , "Geometrical representation of the polarization of a plane electromagnetic wave " Proc Inst Radio Engrs **39**, 540–544 (1951)

[3] Born, M and Wolf, E , *Principles of Optics* (Pergamon Press, New York, 1959), pp 29–31

[4] Schurcliff, W A , *Polarized Light* (Harvard University Press, Cambridge, Mass , 1962) pp 95–99

[5] Drucker, D C and Mindlin, R D , "Stress analysis by three-dimensional photoelastic methods," J Appl Phys **11**, 724–732 (1940)

[6] Drucker, D C , "The photoelastic analysis of transverse bending of plates in the standard transmission polariscope," J Appl Mech **10**, A161–164 (1942)

[7] Franz, G and Teepe, W , "Beitrag zur spannungsoptischen untersuchung von schalen," *Selected Papers on Stress Analysis* (Chapman and Hall Ltd , London, 1961), pp 50–57

MGD Space Propulsion System for Lunar Missions

FRED SPINDLER* AND KENNETH WANG†
Curtiss-Wright Corporation,
Wood-Ridge, N J

IN a recent paper[1] Brown and Nicoll have made a mission study of arcjet and ion engines for lunar ferry missions The calculations indicated that both engines offer payload capabilities superior to the chemical and nuclear rocket propulsion systems, particularly in the case of multitrip ferry missions The present study of the mission capability for an MGD propulsion system also shows the advantage in using it for lunar ferry missions Compared with either an ion engine or arc-jet engine the MGD propulsion system yields either shorter trip duration or larger payload for equal power/weight ratio Thus, an integrated MGD space propulsion system needs to be investigated as a promising system for space exploration

In order for the results of calculation to be meaningful and comparable, a mission profile identical to that described in Ref 1 is adopted

Starting with the characteristics of the MGD propulsion system, the propulsion efficiency is obtained from the theoretical analysis of Ref 2 In Fig 1, the efficiency of the MGD propulsor is presented together with those of the ion engine and arcjet for comparison Then, for a given propulsion time the specific weight of vehicle in lb/kw can be found from the simplified rocket equation for gravity free space For a particular propulsion system the specific weights for the space vehicle components such as guidance system, structure, fuel storage, etc , can be estimated and the specific fuel weight calculated for a given I_{sp}

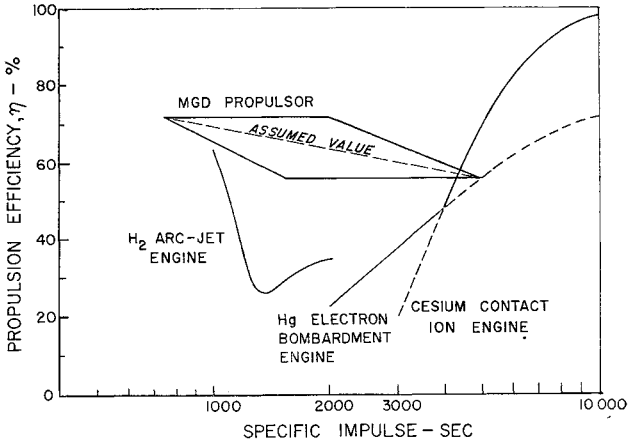

Fig 1 Comparative electric propulsion performance

Finally, the specific payload weight is obtained by subtracting the sum total of these specific weights from the specific weight of vehicle Repeated calculations for various propulsion times and specific impulse values yields a series of parametric mission performance curves showing payload fraction and power to weight ratio

In Fig 2 the payload capabilities of MGD propulsion for a round trip lunar mission are presented together with results of Ref 1 for comparison purposes The specific weights for the space vehicle components adapted in the calculations are as follows: 1) power conversion system weight, 7 lb/kw for the 1–10 mw power range; 2) power conditioning system weight, 3 lb/kw (power transmission lines, switchgear, controls, starting devices, and any requirements for power transformation or rectification); 3) propulsion system weight, 1 lb/kw; 4) guidance and control system weight = 0 3% W_o (initial weight); 5) structural weight of spacecraft = 5% of empty vehicle weight except fuel storage weight; 6) propellant weight = (propulsion time × thrust)/(I_{sp} × power); and 7) propellant storage and feed system weight = 12% of propellant weight

It can be seen that the mission capability of the MGD propulsion system lies approximately midway between that of the arcjet and the ion engine The advantages of the MGD

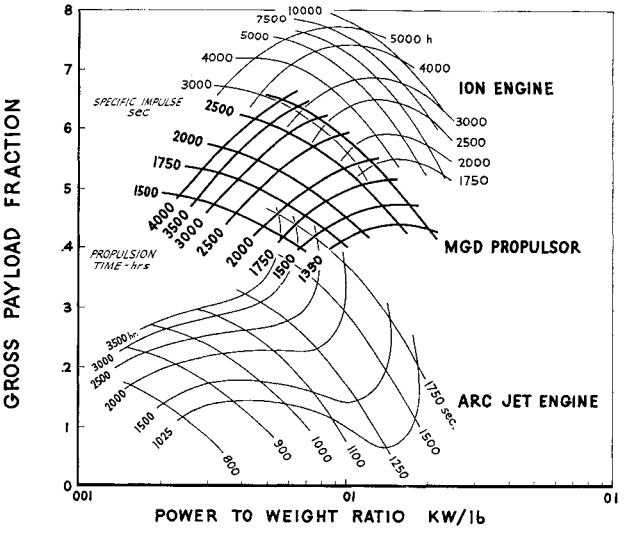

Fig 2 Payload capabilities for round-trip lunar missions

Received October 4, 1963

* Senior Engineer, Advanced Energy Conversion Department, Wright Aeronautical Division

† Project Manager, Advanced Energy Conversion Department, Wright Aeronautical Division Member AIAA